

Notice: This manuscript has been authored by UT-Battelle, LLC, under Contract No. DE-AC0500OR22725 with the U.S. Department of Energy. The United States Government retains and the publisher, by accepting the article for publication, acknowledges that the United States Government retains a non-exclusive, paid-up, irrevocable, world-wide license to publish or reproduce the published form of this manuscript, or allow others to do so, for the United States Government purposes. The Department of Energy will provide public access to these results of federally sponsored research in accordance with the DOE Public Access Plan (<http://energy.gov/downloads/doe-public-access-plan>).

Ionic control over ferroelectricity in 2D layered van der Waals capacitors

Sabine M. Neumayer¹, Mengwei Si², Junkang Li², Pai-Ying Liao², Lei Tao^{3,4}, Andrew O'Hara³, Sokrates T. Pantelides^{3,5}, Peide D. Ye², Petro Maksymovych¹, Nina Balke^{1,6*}

¹ Center for Nanophase Materials Sciences, Oak Ridge National Laboratory, Oak Ridge, 37831 TN, USA
E-mail: balken@ornl.gov

² Birck Nanotechnology Center and School of Electrical and Computer Engineering, Purdue University, West Lafayette, Indiana 47907, USA

³ Department of Physics and Astronomy, Vanderbilt University, Nashville, Tennessee 37235, USA

⁴ University of Chinese Academy of Sciences & Institute of Physics, Chinese Academy of Sciences, Beijing 100190, China

⁵ Department of Electrical Engineering and Computer Science, Vanderbilt University, Nashville, Tennessee 37235, USA

⁶ Department of Materials Science and Engineering, North Carolina State University, Raleigh NC 27695-7907, USA

*Corresponding author:
Nina Balke, ninabalke@ncsu.edu

KEYWORDS

Van der Waals materials, interfaces, metal thiophosphates, ferroelectricity, ionic conductivity, polarization switching, ferroelectric capacitor

The van der Waals layered material CuInP_2S_6 features interesting functional behavior, including the existence of four uniaxial polarization states, polarization reversal against the electric field through Cu ion migration, a negative-capacitance regime, and reversible extraction of Cu ions. At the heart of these characteristics lies the high mobility of Cu ions, which also determines the spontaneous polarization. Therefore, Cu migration across the lattice results in unusual ferroelectric behavior. Here, we demonstrate how the interplay of polar and ionic properties provides a path to ionically controlled ferroelectric behavior, achieved by applying selected DC voltage pulses and subsequently probing ferroelectric switching during fast triangular voltage sweeps. Using current measurements and theoretical calculations,

we observe that increasing DC pulse duration results in higher ionic currents, the build-up of an internal electric field that shifts polarization loops, and an increase in total switchable polarization by ~50% due to the existence of a high polarization phase which is stabilized by the internal electric field. Apart from tuning ferroelectric behavior by selected square pulses, hysteretic polarization switching can even be entirely deactivated and reactivated, resulting in three-state systems where polarization switching is either inhibited or can be performed in two different directions.

1. INTRODUCTION

The multifunctionality of van der Waals (vdW) layered copper indium thiophosphate CuInP_2S_6 (CIPS), including ferroelectricity,^{1,4} negative electrostriction,⁵⁻⁶ and ion conductivity,⁷⁻⁹ provides interesting opportunities for nanoelectromechanical devices and information storage. The layered vdW structure¹⁰⁻¹¹ allows cleavage of the crystal into ultrathin flakes that are still electromechanically active down to tens of nm in thickness.¹²⁻¹³ The cleaved surfaces of these quasi-two-dimensional (2D) materials provide clean interfaces without dangling bonds and are therefore highly suitable for creating heterostructures with 2D materials such as MoS_2 or graphene to further enhance functionality, *e.g.* in ferroelectric field-effect transistors.¹⁴ Below the Curie temperature of ~310 K, CIPS is ferroelectric with a polarization of typically 2.5 - 5 $\mu\text{C}/\text{cm}^2$ observed in hysteresis loops measured on micrometer scale electrodes.^{1, 15} Although the polarization is lower than for other ferroelectrics, such as perovskite oxides, a relatively high electrostrictive coefficient leads to comparable longitudinal piezoelectric output.⁵⁻⁶

It was recently discovered that the polar properties of CIPS are more complex on the nanoscale. A combination of density functional theory (DFT) calculations and local piezoresponse-force-microscopy (PFM) discovered that there are actually two distinct iso-symmetric polar phases present in CIPS with a theoretical polarization of ~5 $\mu\text{C}/\text{cm}^2$ (low-polarization phase, LP) and ~11 $\mu\text{C}/\text{cm}^2$ (high-polarization phase, HP), in which the Cu ions reside just inside or just outside of the layers, respectively.⁴ As a consequence, the energy potential well as a function of Cu displacement shows a quadruple well instead of the more common double potential well exhibited by other ferroelectric materials. Copper-ion conduction is characterized by an activation energy of 0.73 eV from macroscopic characterization⁷ and 0.71 eV from local characterization,⁸ respectively. This is in good agreement with theory, which shows that the energy barrier for Cu-ion jumps across the vdW gap was calculated to be 0.65 - 0.75 eV in the presence of Cu Frenkel pairs and slightly higher in stoichiometric regions.¹⁶

As a material that exhibits both ferroelectricity and ionic conductivity, CIPS has the not-so-common property that the same atomic species, Cu, is responsible for both the short-range displacements that determine the polarization in the ordered, ferroelectric state below T_c ^{1,4} and the long-range ionic current across layers and van der Waals gaps,⁷⁻⁸ which is viewed as a disordered state. In 1999, Scott pointed out that in materials that feature such a property, at temperatures below T_c , voltage can be used to transition from the ordered ferroelectric state to the disordered state of ionic conductivity using $\text{Ag}_{26}\text{I}_{18}\text{W}_4\text{O}_{16}$ where Ag ions are the mobile species.¹⁷ More specifically, he suggested that for small voltages, the polar atomic displacements can be flipped back and forth within the double-well potential by reversing the field, while at large voltages above a threshold value the energy barrier for displacements between unit cells would be overcome and the ions would move without bound. Therefore, a strong dependence of ferroelectric material properties on voltage amplitude and duration is expected. Indeed, it has been shown that the frequency of electric-field cycles affects polarization switching in CIPS. Most notably, the polarization increases with decreasing frequency of the electric field cycle and the hysteresis loops appear imprinted for high frequency field cycles.⁹ This behavior has been explained by the rotation of ionic defect dipoles rather than by ionic conductivity.⁹ However, it has already been demonstrated that at room temperature, *i.e.*, in the ferroelectric phase, application of voltage pulses can drive the Cu atoms across the vdW gap, which leads to highly unusual polarization reversal processes such as polarization alignment against the applied electric field. This phenomenon has been demonstrated for locally biased measurements with an atomic force microscope (AFM) probe across one vdW gap¹⁸ as well as under biased electrodes across multiple vdW gaps.¹⁶ These observations demonstrate that it is possible to explore the regime of coexisting ferroelectric and ionic properties but it has not been leveraged yet to actively control material functionality, *e.g.*, ferroelectric properties.

In this work, we activate ionic conductivity at room temperature using electric fields and study its impact on ferroelectric switching in CIPS micro-capacitors. After activation, we found that polar and ionic properties co-exist and contribute this to measured currents. Based on current-voltage characteristics we can distinguish between ionic and polarization-switching currents and study the symbiotic interplay of polarization and ionic conductivity. We find that the presence of increasing ionic currents alters the timing and intensity of switching peaks, which in turn leads to evolving polarization loops, demonstrating direct control of polarization loops by ionic currents. These changes in the polarization hysteresis can be explained by DFT calculations in terms of an internal electric field that builds up as ionic currents drive an increasing number of Cu ions to the top CIPS-electrode interface, while an increasing number of CIPS layers at the bottom of the stack are depleted of Cu ions and become metallic, maintaining the circuit integrity. Moreover, the internal field favors the HP state over the LP state in the direction of the electric field, which

explains the increase in measured polarization. In the extreme case at higher voltages, ionic conduction was found to entirely suppress ferroelectric hysteretic switching, a process that is reversible, allowing turning the ferroelectric characteristic on and off.

2. RESULTS AND DISCUSSION

2.1 Measured relationship between ionic currents and ferroelectric behavior

Square and triangular voltage, V , pulses are applied to the top electrode of a ferroelectric CIPS capacitor (see schematic in Fig. 1(a)) via micromanipulators to activate ionic currents and study their influence on the switching behavior in subsequent fast triangular voltage sweeps. In a first step, we applied a square pulse of varying duration followed by triangular V sweeps on a pristine CIPS capacitor and recorded the resulting currents, I . Figure 1(b) shows the voltage, V , waveform consisting of DC pulses of 4, 10, 20, 100, 200, 400, 500, 600, 800, or 900 ms duration at an amplitude of -4 V. Subsequently, the ferroelectric behavior was probed by two triangular V sweeps of 10 ms duration each, as typically performed for ferroelectric characterization. The amplitudes of the DC pulse and the triangular V sweeps of 4 V were chosen to clearly exceed the coercive voltages that lead to ferroelectric switching in this ~185 nm thick sample. Figure 1(c) shows the currents measured during the entire duration of all DC voltage pulses. For each DC voltage pulse, a polarization switching current peak is detected within the first 2 ms. For voltage pulses longer than 100 ms, significant current is detected, which grows exponentially to exceed the specific current measurements limits of -256 nA for pulses longer than 400 ms. This second current contribution is assigned to an ionic current indicating Cu ions move beyond the unit cell. It is evident that the DC voltage step can be used to control the amount of ionic current. The currents at the beginning and end of each DC voltage pulse are shown in detail in Fig. S1. Figure 1(d) depicts the currents during the subsequent two triangular voltage sweeps at 100 Hz. Up to 100 ms duration of the preceding DC voltage pulse, only polarization switching current peaks corresponding to ferroelectric displacements are observed. There are no switching peaks at the negative voltage in the first cycle as the system is already switched to a positive polarization orientation due to the negative polarity of the DC voltage pulse. This feature agrees with standard ferroelectric behavior. For longer DC voltage pulses, additional current contributions for $V < 0$ become visible, indicating ionic current contributions during 100 Hz field cycling. However, the current peak assigned to polarization switching for $V < 0$ is still visible. It shall be noted that the situation reverses for positive DC pulses that lead to positive ionic currents during the DC pulse and the triangular V sweep (Fig. S2). The total current, I , can be divided into two types corresponding to their origin: (i) ionic currents proportional to the applied voltage for negative voltage polarity and (ii) switching current peaks for positive and negative voltage polarity originating from charge redistribution at the electrodes after polarization reversal.

Separating these current contributions allows the study of ferroelectric switching in the presence of ionic currents.

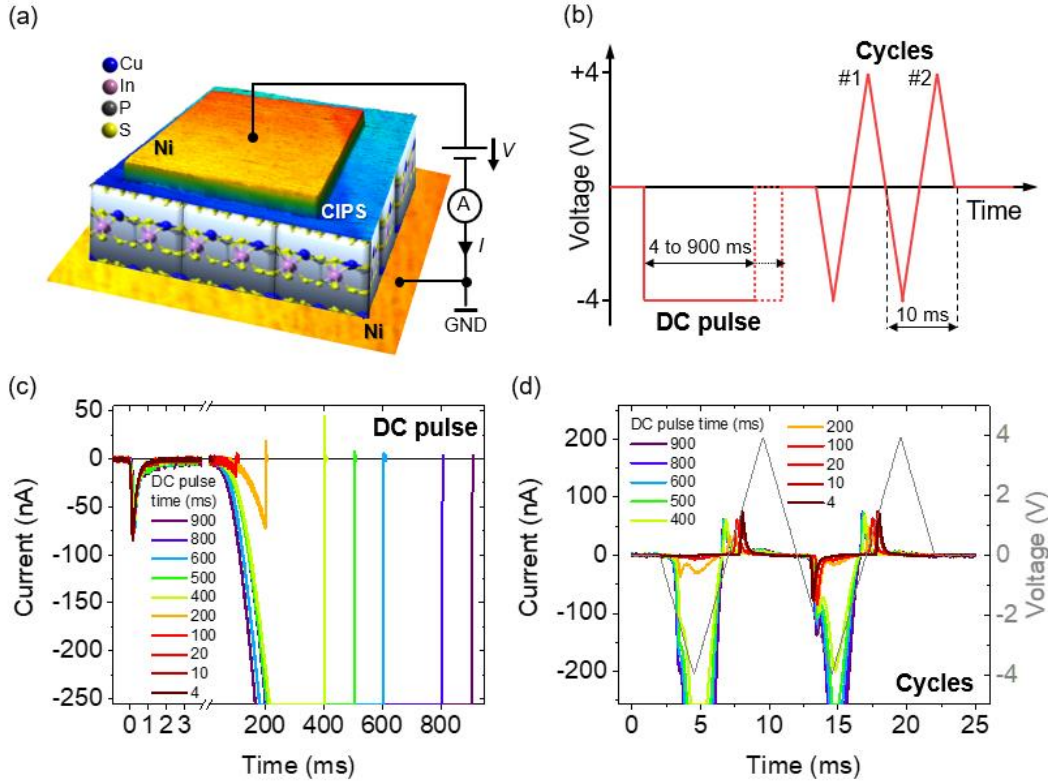


Fig. 1. (a) Schematic depiction of experimental setup and (b) applied voltage sequence showing -4 V DC voltage pulses with a duration of 4 to 900 ms (10 steps) preceding two triangular voltage cycles between ± 4 V of 10 ms duration each. (c) Currents measured during DC pulses of varying duration. The square voltage pulses were turned on at 0 s. (d) Currents measured during triangular cycles. Labels in legends refer to DC pulse duration in ms.

In the following, we focus on the analysis of the current signal during the triangular voltage sweeps. As shown in Fig. 1(d), ferroelectric and ionic current contributions are visible. To separate these contributions, a four-peak fitting method was applied to separate the two polarization switching peaks and the ionic contribution during the second triangular voltage sweep. The second cycle was chosen for the analysis since the first cycle did not describe the full polarization hysteresis loops. However, it is visible in Fig. 1(d) that the ionic current contribution is reduced between the first and second cycle, which we will address later. The fitted ionic current contribution as well as the switching current peaks after the current separation are shown in Fig. 2(a) and 2(b), respectively. The fits are shown in detail in Fig. S3. The corresponding

hysteresis loops of polarization obtained by integrating the polarization switching current peaks in Fig. 2(c) are calculated via $P = -\frac{1}{A} \int I(t)dt$, where t is the time and A is the area of the electrode. Note that the currents measured at the electrode occur in response to screening the ferroelectric polarization, where a negative current peak corresponds to ferroelectric switching for a more positive polarization state. The polarization hysteresis loops are centered in Fig. 2(c) for better clarity. This is an accepted procedure since only relative polarization changes are measured.

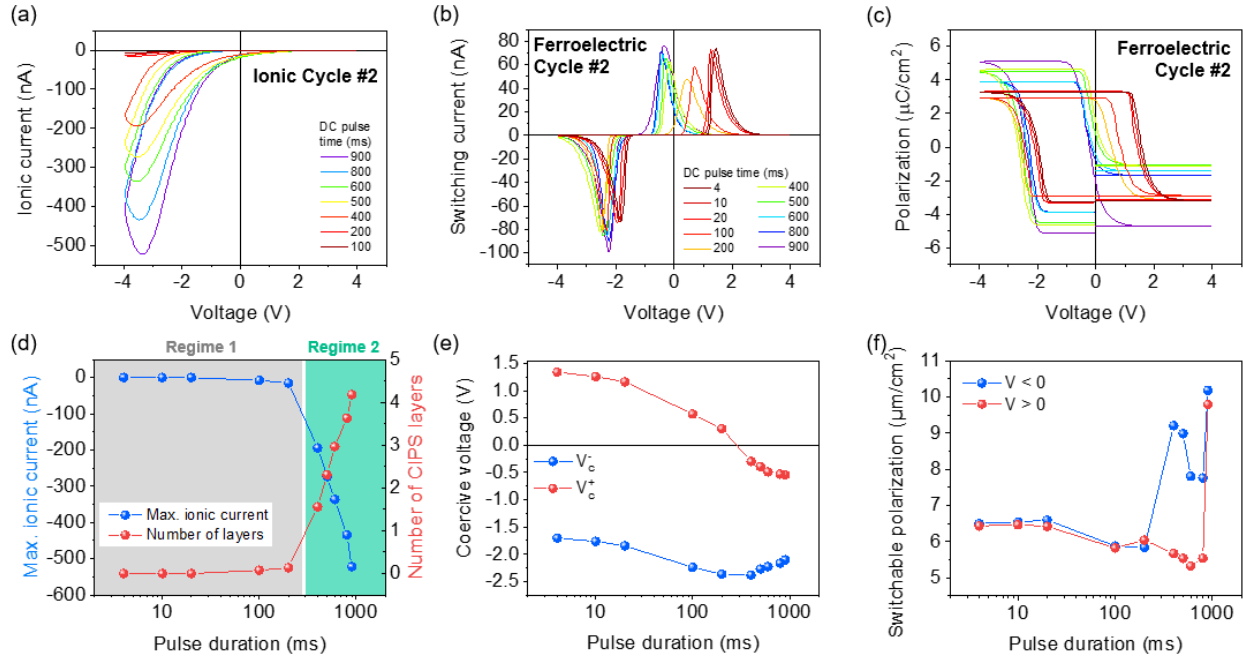


Fig. 2. (a) Ionic current during triangular sweeps for the second cycle extracted from total current fitting. (b) Switching current calculated from total current fitting. (c) Polarization hysteresis loops calculated from (b). (d) Maximum ionic current as a function of DC voltage pulse duration and corresponding number of CIPS layers below the electrode area contributing to the ionic charge. Gray and green backgrounds indicate two regimes with significantly different amounts of ionic current. (e) Coercive voltages extracted from current peaks in panel (b). (f) Absolute value of switchable polarization on the left ($V < 0$) and right ($V > 0$) side of the hysteresis loop as a function of pulse duration.

It can be seen that the ferroelectric polarization hysteresis loop is affected by the ionic current. We can identify two regimes determined by the maximum ionic current and ionic charge that can be related to the number of CIPS layers that are needed to provide their Cu ions for electrochemical reactions so that the measured maximum ionic current can be reached (Fig. 2(d)). Details on how the ionic current is related to

ionic charge and number of CIPS layers under the electrode area and the provided the charge are shown in the Supplemental Information (Fig. S4). Two clear regimes with different behavior are highlighted in Fig. 2(d) by shaded backgrounds. The transition between the two different regimes coincides with the amount of charge the Cu from a single layer of CIPS can provide, 0.20 nC, under the assumption that each Cu ion reacts with one electron, as discussed below. In regime 1 up to 200 ms DC voltage duration, no (4 ms, 10 ms, 20 ms) or only minimal (100 ms, 200 ms) ionic currents are detected. In this regime, both coercive voltages shift toward negative voltages indicating the formation of an internal bias field that stabilizes the negative polarization direction (Fig. 2(e)). The direction of the internal bias field is consistent with a positive charge accumulation at the top electrode, which is caused by an accumulation of Cu ions under the influence of the negative DC voltage pulses. The coercive voltage shift is consistent with observations by Zhou et al.⁹ At the same time, the amount of switchable polarization with positive and negative voltages are identical and decrease slightly from 6.6 $\mu\text{C}/\text{cm}^2$ to 5.9 $\mu\text{C}/\text{cm}^2$ (Fig. 2(f)). In regime 2, for DC pulse duration larger than 200 ms, the maximum ionic current during the triangular sweep increases linearly as a function of the logarithmic DC voltage pulse duration and grows >80 nA per 100 ms. In this regime, the positive coercive voltage continues to shift toward more negative voltages and becomes negative itself, while the negative coercive voltage reverses trend and shifts toward more positive voltages. This change is accompanied by asymmetric hysteresis loops (different amount of switchable polarization on each side of the hysteresis loop), which originate due to the increase of the negative polarization P^- . For the longest DC voltage duration of 900 ms, the positive polarization P^+ increases as well, making the polarization hysteresis more symmetric with respect to the polarization axis with an increased switchable polarization of about 10 $\mu\text{C}/\text{cm}^2$. The strong shift of both coercive voltages into the negative voltage regime leads effectively to a loss of remanent polarization reversal. It is also noteworthy that while the polarization hysteresis changes drastically, the area of the polarization loops, related to energy, is fairly constant and ranges between 0.24 J and 0.16 J (Fig. S5).

Next, we discuss the observation of ionic currents during the 100 Hz voltage sweeps. Evidently, generating ionic current during >100 ms DC voltage pulses directly enhances ionic conductivity in the subsequent fast voltage sweeps for the same voltage polarity. We hypothesize that the ionic current is based on an electrochemical reaction of Cu ions at the electrode forming Cu metal. Based on the polarity of the DC voltage pulse, Cu ions accumulate under one of the electrodes (top or bottom) and partially react to Cu metal leading to current flow, $\text{Cu}^+ + e^- \rightarrow \text{Cu}$. In subsequent fast sweeps, ionic currents can be measured because accumulated Cu^+ is readily available at that electrode, which increases the kinetics of the electrochemical reaction. Over time, Cu redistributes, driven by a voltage-induced concentration gradient that minimizes the amount of Cu^+ accumulation under the electrode, leading to a smaller ionic current with

each subsequent cycle as shown in Fig. S6 for 10 cycles measured after DC voltage pulses of 20 ms, 500 ms and 1000 ms duration (Fig. S7). Alternatively, the application of DC voltage pulses can lead to the formation of defects, such as Cu vacancies and Frenkel pairs, which lower the energy barrier to cross the vdW gap.¹⁶ In this scenario, we have to assume that these defects are not stable over time or under continuous cycling.

2.2 Theoretically calculated impact of ion accumulation and depletion on ferroelectric hysteresis

We now turn to the results of theoretical calculations based on DFT aimed to explore the connection between polarization hysteresis loops and ionic current in CIPS. We employed a stack of six CIPS layers with Ni electrodes (three layers of Ni atoms) using an in-plane unit cell that contains four formula units per CIPS layer. To simulate the effect of negative DC voltage pulses applied to the top electrode during the experiment, we start with a stoichiometric CIPS stack where all Cu atoms are at the bottom of the layers in the -LP state (Fig. 3(a)) and move the Cu sheets upwards across layers and vdW gaps, going through multiple negative and positive polarization states (Fig. 3(b-h)). At each point, the system is fully relaxed. This process results in the formation of Cu-depleted CIPS layers at the bottom electrode and Cu accumulation underneath the top electrode, simulating Cu redistribution under externally applied fields. The number of empty CIPS layers vs. the number of fully stoichiometric CIPS layers in the stack are expressed by m and n , respectively, and the stack can be described by the general form of $\text{Ni}/m \text{ InP}_2\text{S}_6/n \text{ CuInP}_2\text{S}_6/\text{Cu}/\text{Ni}$ (Fig. 3(i)).

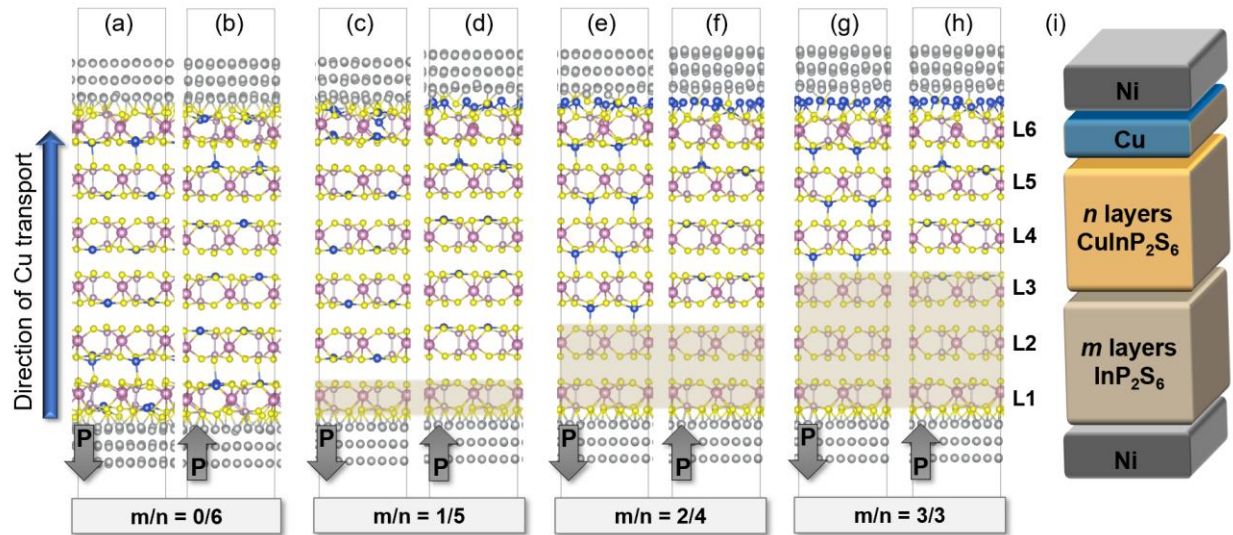


Fig. 3. Stack of six CIPS layers with Ni-layer top and bottom electrodes at various stages of concerted, upward Cu motion. Relaxed structure of CIPS stack for (a,b) no empty CIPS layers ($m = 0$), (c,d) one empty CIPS layer ($m = 1$), (e,f) two empty CIPS layers ($m = 2$), and (g,h) three empty CIPS layers ($m = 3$) for the downward and upward polarized state, respectively. Cu-free CIPS layers are highlighted in beige. (i)

General schematic of CIPS stack including Cu-empty and fully stoichiometric CIPS layers and accumulated Cu under the top electrode for $m > 0$.

Noteworthy points are as follows. In the initial state, when all Cu atoms are in a negative polarization state, they occupy the -LP state, but Cu atoms in the top layer (L6) and the bottom two layers (L1/L2) undergo substantial relaxations (Fig. 3(a)). When the Cu ions are moved across the layers to a positive polarization state (Fig. 3(b)), they occupy the +LP state, but the relaxations now are substantial in the top two layers (L5/L6). In the next step (Fig. 3(c)), the Cu sheets are moved across the vdW to negative-polarization states with the polarization aligned against the external electric field that in principle is driving the upward motion of the Cu ions. We now have an empty CIPS layer at the bottom and one Cu sheet under the top Ni electrode. The topmost Cu sheet does not spontaneously electroplate on the Ni electrode. Instead, S atoms tend to bond to Ni atoms across the interface. We checked that electroplating indeed does not take place by placing the Cu atoms on the Ni surface, but upon relaxation, Cu retreated to the nearest CIPS layer (a single CIPS Cu sheets corresponds to only $\frac{1}{4}$ of the Cu atoms needed to form a Cu monolayer on Ni). In the next step (Fig. 3(d)), when we move the Cu sheets across the layers one more time and Cu atoms from two CIPS layers are at the top electrode interface, partial electroplating begins. In the next step, Fig. 3(e), we move the Cu sheets across the gaps again, leaving two empty layers at the bottom. For the first time, Cu atoms in the “bulk” layers spontaneously acquire -HP positions, while in the subsequent step (Fig. 3(f)), the relaxed Cu position is on the +LP polarization state, which is also true for the configuration with one more empty CIPS layer (Fig. 3(g,h)).

In order to determine the metallic or insulating nature of the CIPS layers as we proceed through the evolution depicted in Fig. 3, we calculated the projected densities of states (PDOS) for all the layers in each of the eight stacks. The most important finding is that the Cu-depleted CIPS layers at the bottom become metallic while the stoichiometric CIPS layers remain insulating. This result is shown for the example of two empty CIPS layers ($m/n = 2/4$) in Fig. 4(a). The two bottom layers (L1/L2) clearly show metallic character while the layers containing Cu (L3-L6) maintain their insulating character. The PDOS for all configurations shown in Fig. 3 are shown in Fig. S8. We note that in a physical system with a very large number of CIPS layers, after emptying four CIPS layers at the bottom and electroplating a full monolayer of Cu on the top electrode, we effectively start again from the configuration of Fig. 3(a) where we have a stack of stoichiometric CIPS layers between metallic electrodes, which are formed by Ni/InP₂S₆ at the bottom and Ni/Cu at the top. This result is enabling us to compare additional theoretical results obtained from the configurations in Fig. 3 with the experimental data. We note that metallicity is not present in the

Cu-free equilibrium phase of $\text{In}_{4/3}\text{P}_2\text{S}_6$ (Fig. S9). Here, the metallic behavior arises due to the Cu-depleted layers in non-stoichiometric InP_2S_6 .

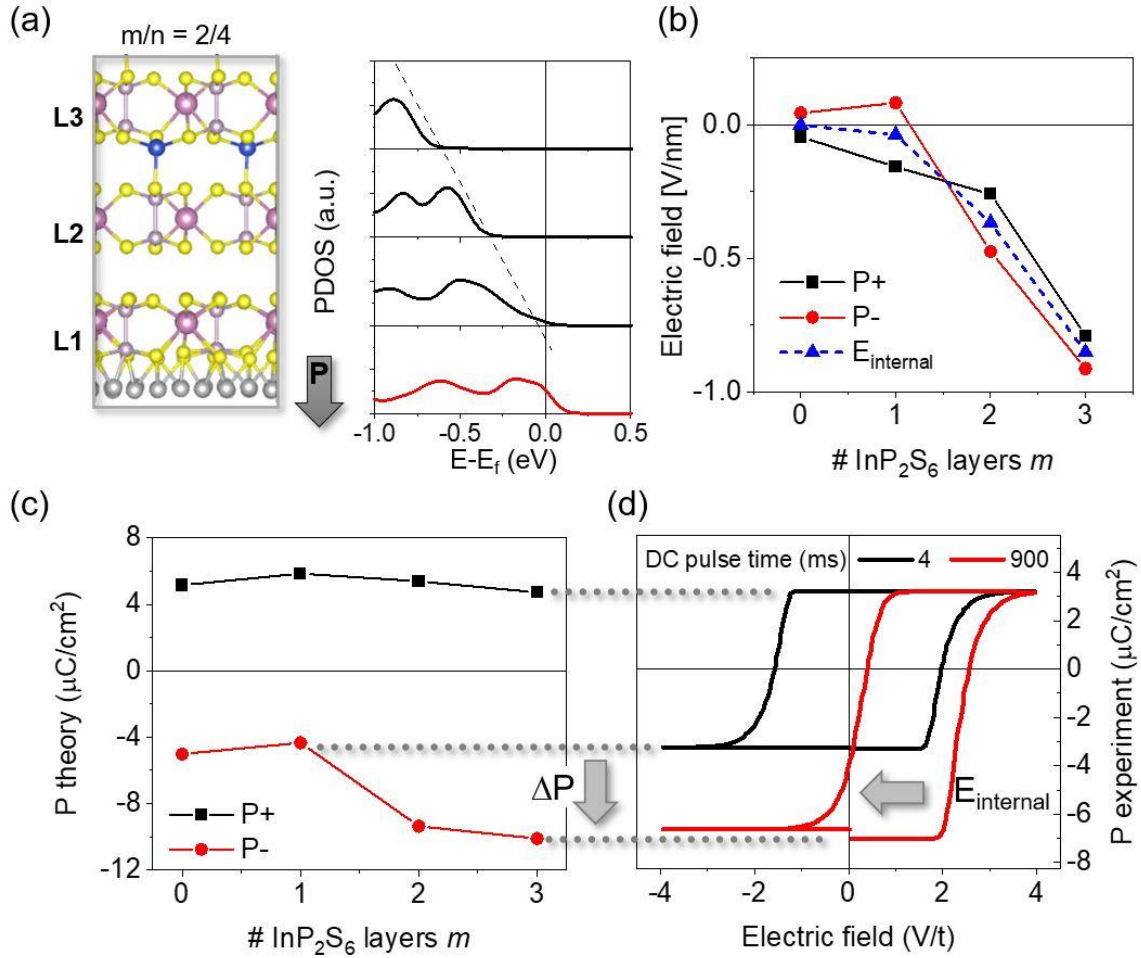


Fig. 4. (a) Layer-projected DOS (PDOS) in the $m/n=2/4$ stack of Fig. 3(e) showing metallic nature of Cu-free layer L2. Electrically insulating layers are drawn in black, conductive layers are drawn as red lines. Layer L1 and L6 are omitted as they are fully metallic due to contact doping in all cases. The slope of dashed line corresponds to value of internal electric field that arises from Cu migration to the top electrode. (b) Progression of calculated internal field for eight stacks of Fig. 3 for each pair of polarization states and average of the two. (c) Calculated average polarization values per layer in eight stacks of Fig. 3. (d) Experimental polarization loops for DC voltage pulses of 4 ms and 900 ms duration.

The PDOS plots also allow us to determine the internal electric field, E_{internal} , that is generated by the movement of Cu atoms leaving empty layers at the bottom and placing Cu atoms at the top interface. We obtain the electric field in each stack by tracing the top of the valence bands through the insulating CIPS

layers (dashed line in Fig. 3(a); see also Fig. S8). This trace is effectively the macroscopic electrostatic potential that is generated by the empty layers at the bottom and the Cu atoms at the top interface. The slope of the linear trace is the corresponding $E_{internal}$. The potentials are shown in Fig. S10(a) while the resulting electric fields as the system evolves are shown in Fig. 4(b). The blue points correspond to the $E_{internal}$, which is proportional to the number of empty CIPS layers, m . The sign of this field corresponds to pushing Cu atoms downward, *i.e.*, it opposes the external electric field that pushes Cu atoms upward.

Using the results obtained from the calculations for Fig. 3, we derived the actual polarization values for each of the stacks. We used the calculated Cu displacements in each of the stoichiometric layers in the stack, averaging over the layers and then using the polarization-versus-Cu-displacement curve reported in Ref. ⁴ for bulk CIPS. The average polarization versus average Cu displacements are shown in Fig. S10(b) and the extracted polarization values as functions of the number of empty CIPS layers, m , are shown in Fig. 4(c). As described earlier, the positive +LP state is unaffected by the empty CIPS layers whereas $E_{internal}$ stabilizes the -HP state instead of the -LP state for two or more empty CIPS layers, which effectively doubles the negative polarization value.

The information of $E_{internal}$ and polarization as functions of the number of empty CIPS layers can be used to understand the experimentally observed changes in the polarization hysteresis loops. As an example, we show the polarization for a DC voltage pulse duration of 4 ms and 900 ms as a function of field (instead of voltage) in Fig. 4(d). First, the $E_{internal}$ is negative, which matches the predicted direction. A negative internal field stabilizes the negative polarization state and needs to be overcome by the externally applied field. Therefore, the polarization loop effectively shifts towards higher positive fields. However, absolute values of the $E_{internal}$ cannot be compared between theory and experiment because the sample thickness is unknown and the formation of conductive empty CIPS layers would effectively change the ferroelectric sample thickness during the experiment. Second, the experimentally observed polarization values are slightly smaller than the theoretically predicted ones. Based on the comparison of theory and experiment, the switchable polarization in the absence of ionic conduction (no empty CIPS layers) is 10.2 $\mu\text{C}/\text{cm}^2$ and 6.4 $\mu\text{C}/\text{cm}^2$, respectively. In the presence of ionic conduction with three empty CIPS layers, the switchable polarization increases to 14.8 $\mu\text{C}/\text{cm}^2$ in theory and 9.8 $\mu\text{C}/\text{cm}^2$ in the experiment. These values correspond to 46% and 53% increases, respectively. Therefore, we conclude qualitatively that the stabilization of the -HP state is the origin of the observed polarization increase. The asymmetry between positive and negative polarization values could also explain the difference in switchable polarization for intermediate DC voltage-pulse duration resulting in non-closed hysteresis loops (Fig. 2(c)).

2.3. Deactivation and reactivation of hysteretic behavior

It is natural to assume that with higher electric fields or longer durations, the Cu ions within CIPS are completely disordered and no ferroelectric phase persists. In order to explore if that regime can be reached, we repeated the measurement on a different capacitor. Initially, we observed a hysteresis loop typical for CIPS (Fig. 6(a)) with a polarization around $\pm 5 \mu\text{C}/\text{cm}^2$ and a V_c^- around -3 V and a V_c^+ around +5 V. Applying two high voltage pulses of -10 V for 2 and 3 s before the triangular V sweep results in the disappearance of hysteretic behavior (Fig. 6(b)). It is noteworthy that after a V pulse of +10 V for 1 s, the hysteretic state was restored with polarization and coercive voltage values similar to the initial state (Fig. 6(c)). Evidently, deactivation and recovery of ferroelectric switching through high-amplitude voltage pulses provides a path to toggle between hysteretic and non-hysteretic states. The highly reversible nature of Cu redistribution by external fields agrees well with the reversible extraction and reinsertion of Cu from and into CIPS found at higher temperatures.⁸ This remarkable reversibility provides exciting opportunities for memory devices beyond binary limitations. In such devices, information could be encoded in three events: (i) switching from positive to negative P , (ii) switching from negative to positive P , and (iii) no polarization switching within the same voltage range.

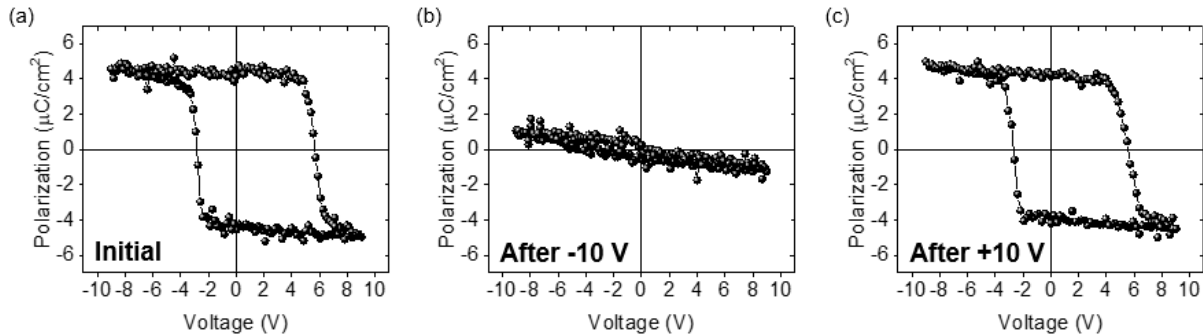


Fig. 5. Recovery of switching with voltage. Polarization loops of CIPS capacitor (a) initially, (b) after applying a -10 V/ 2+3 s voltage pulses, and (c) after applying a +10 V/ 1 s pulse.

3. CONCLUSIONS

We demonstrate ionic control of ferroelectric behavior in CuInP_2S_6 capacitors where the position of Cu ions with respect to the layers determines the polarization while simultaneously exhibiting a high mobility.

Dependent on the duration of DC voltage pulses, ionic currents become measurable and modify ferroelectric characteristics in subsequent triangular voltage sweeps as measured experimentally. The process of Cu transport is simulated theoretically and the consequences of Cu-free CIPS layers and Cu accumulation under the electrodes on internal electric fields and polarization is explored. Increasing ionic currents, which is equivalent to the formation of an inhomogeneous Cu distribution under the electrodes, lead to internal electric fields that point opposite to the field driving the ionic motion. Therefore, the polarization hysteresis loops become imprinted. In addition, the high- instead of the low-polarization phase is stabilized in the direction of the internal electric field, with the Cu ions displaced slightly into the vdW gaps. This feature doubles the amount of polarization for one polarity, which can explain the ~50% increase in switchable polarization. The interplay of ionic and polar properties can be used to fine-tune ferroelectric characteristics or to fully deactivate and reactivate hysteretic behavior, which provides the exciting opportunity for a three-state ferroelectric capacitor showing either switching between positive and negative polarization states or non-hysteretic characteristics. Moreover, we expect similar phenomena to manifest in other ferroelectric materials where the ionic sublattice that determines polar properties consists of the most mobile ionic species in that compound.

4. METHODS

4.1 Experimental

CIPS crystal growth was obtained through a solid-state reaction by mixing powders of the four elements and annealing in vacuum at 600 °C for 2 weeks. Scotch tape-based exfoliation was used to transfer flakes onto a 20 nm Ni/90 nm SiO₂/Si substrate. Top electrodes were fabricated using electron-beam lithography, electron-beam evaporation, and a lift-off process. The electrode size was 20×20 μm with a thickness of 70 nm (20 nm Ni + 50 nm Au). The capacitor fabrication process is described in detail in Si et al.¹⁵ Three different capacitor sample were used in this work with thicknesses of the CIPS layers of approximately 185 nm (Fig.1 and 2), 420 nm (Fig. S6 and S7) and 500 nm (Fig.5). These values were calculated from the measured coercive voltages and the coercive field of 8.9 mV/nm known from previous measurement on a Ni/CIPS/Ni capacitor sample where the CIPS thickness was known.¹⁴

The micromanipulator setup consisted of a Cascade Microtech probing station equipped with a Keysight B1500A Semiconductor Device Analyzer and a Radiant Technologies Precision RT66C precision materials analyzer for *I-V* and *P-V* measurements. An Agilent 33220A arbitrary wave generator and a Tektronix TDS5032B oscilloscope are used for the pulsed *I-V* measurements.

The full waveform used for the DC voltage pulse experiment shown in Fig. 1 consisted of the square pulse, a first triangular cycle starting with negative voltages and a second triangular cycle. The triangular cycles were applied immediately after the square pulse. The triangular I-V curves in Fig. 1 and Fig. 2 were acquired at 100 Hz and the polarization loops in Fig. 5 were measured at 200 Hz.

4.2 Theoretical

The DFT calculations in this study were performed with the Vienna Ab-initio Simulation Package (VASP)¹⁹ where the core-valence-electron interactions are described via the projected-augmented-wave (PAW) method.²⁰⁻²¹ The wave functions were expanded in a plane-wave basis using a 400 eV energy cutoff. Exchange-correlation effects were described using the Perdew-Burke-Ernzerhof²² generalized gradient approximation including van der Waals corrections via Grimme's DFT-D3 method with Becke-Johnson (BJ) damping.²³⁻²⁴ The system was modeled using a supercell containing 6 layers of (2×1) CuInP₂S₆ and 3 layers of $(4 \times 3\sqrt{2})$ Ni(111) on both sides of CIPS with a vacuum layer of 15 Å. All atoms were fully relaxed until the net force is smaller than 0.02 eV/Å.

ACKNOWLEDGEMENTS

Experiments and analysis were supported by the U.S. Department of Energy (DOE), Office of Science, Basic Energy Sciences, Materials Sciences and Engineering Division. The SPM experiments were conducted at the Center for Nanophase Material Sciences, which is a U.S. DOE Office of Science User Facility. Theory and analysis, performed at Vanderbilt University, was supported by the U.S. DOE, Office of Science, Basic Energy Sciences, Materials Sciences and Engineering Division grant No DE-FG02-09ER46554 and the McMinn Endowment. Computations were performed at the National Energy Research Scientific Computing Center (NERSC), a U.S. Department of Energy Office of Science User Facility operated under Contract No. DE-AC02-05CH11231.

REFERENCES

1. Maisonneuve, V.; Cajipe, V.; Simon, A.; Von Der Muhll, R.; Ravez, J., Ferrielectric ordering in lamellar CuInP2S6. *Physical Review B* **1997**, *56* (17), 10860-10868.
2. Liu, F.; You, L.; Seyler, K. L.; Li, X.; Yu, P.; Lin, J.; Wang, X.; Zhou, J.; Wang, H.; He, H., Room-temperature ferroelectricity in CuInP2S6 ultrathin flakes. *Nature Communications* **2016**, *7*, 12357.
3. Susner, M. A.; Belianinov, A.; Borisevich, A.; He, Q.; Chyasnavichyus, M.; Demir, H.; Sholl, D.; Ganesh, P.; Abernathy, D.; McGuire, M. A.; Maksymovych, P., High-Tc Layered Ferrielectric Crystals by Coherent Spinodal Decomposition. *ACS Nano* **2015**, *9* (12), 12365–12373.
4. Brehm, J. A.; Neumayer, S. M.; Tao, L.; O'Hara, A.; Chyasnavichus, M.; Susner, M. A.; McGuire, M. A.; Kalinin, S. V.; Jesse, S.; Ganesh, P.; Pantelides, S. T.; Maksymovych, P.; Balke, N., Tunable quadruple-well ferroelectric van-der-Waals crystals. *Nature Materials* **2020**, *19* (1), 43-48.
5. Neumayer, S. M.; Eliseev, E. A.; Susner, M. A.; Tselev, A.; Rodriguez, B. J.; Brehm, J. A.; Pantelides, S. T.; Panchapakesan, G.; Jesse, S.; Kalinin, S. V.; McGuire, M. A.; Morozovska, A. N.; Maksymovych, P.; Balke, N., Giant negative electrostriction and dielectric tunability in a van der Waals layered ferroelectric. *Physical Review Materials* **2019**, *3* (2), 024401.
6. You, L.; Zhang, Y.; Zhou, S.; Chaturvedi, A.; Morris, S. A.; Liu, F.; Chang, L.; Ichinose, D.; Funakubo, H.; Hu, W.; Wu, T.; Liu, Z.; Dong, S.; Wang, J., Origin of giant negative piezoelectricity in a layered van der Waals ferroelectric. *Science Advances* **2019**, *5*, eaav3780.
7. Maisonneuve, V.; Reau, J. M.; Dong, M.; Cajipe, V. B.; Payen, C.; Ravez, J., Ionic conductivity in ferroic CuInP2S6 and CuCrP2S6. *Ferroelectrics* **1997**, *196* (1), 257-260.
8. Balke, N.; Neumayer, S. M.; Brehm, J. A.; Susner, M. A.; Rodriguez, B. J.; Jesse, S.; Kalinin, S. V.; Pantelides, S. T.; McGuire, M. A.; Maksymovych, P., Locally Controlled Cu-Ion Transport in Layered Ferroelectric CuInP2S6. *ACS Applied Materials & Interfaces* **2018**, *10* (32), 27188-27194.
9. Zhou, S.; You, L.; Chaturvedi, A.; Morris, S. A.; Herrin, J. S.; Zhang, N.; Abdelsamie, A.; Hu, Y.; Chen, J.; Zhou, Y.; Dong, S.; Wang, J., Anomalous polarization switching and permanent retention in a ferroelectric ionic conductor. *Materials Horizons* **2020**, *7* (1), 263-274.
10. Susner, M. A.; Chyasnavichyus, M.; McGuire, M. A.; Ganesh, P.; Maksymovych, P., Metal Thio- and Selenophosphates as Multifunctional van der Waals Layered Materials. *Advanced Materials* **2017**, *29* (38), 1602852.
11. Maisonneuve, V.; Evain, M.; Payen, C.; Cajipe, V. B.; Molinie, P., Room-Temperature Crystal-Structure of the Layered Phase Cu(I)In(III)P2S6. *Journal of Alloys and Compounds* **1995**, *218* (2), 157-164.
12. Chyasnavichyus, M.; Susner, M. A.; Ievlev, A. V.; Eliseev, E. A.; Kalinin, S. V.; Balke, N.; Morozovska, A. N.; McGuire, M. A.; Maksymovych, P., Size-effect in layered ferrielectric CuInP2S6. *Applied Physics Letters* **2016**, *109* (17), 172901.
13. Liu, F.; You, L.; Seyler, K. L.; Li, X.; Yu, P.; Lin, J.; Wang, X.; Zhou, J.; Wang, H.; He, H.; Pantelides, S. T.; Zhou, W.; Sharma, P.; Xu, X.; Ajayan, P. M.; Wang, J.; Liu, Z., Room-temperature ferroelectricity in CuInP2S6 ultrathin flakes. *Nature Communications* **2016**, *7*, 12357.
14. Si, M.; Liao, P. Y.; Qiu, G.; Duan, Y.; Ye, P. D., Ferroelectric Field-Effect Transistors Based on MoS2 and CuInP2S6 Two-Dimensional van der Waals Heterostructure. *ACS Nano* **2018**, *12* (7), 6700-6705.

15. Si, M.; Saha, A. K.; Liao, P. Y.; Gao, S.; Neumayer, S. M.; Jian, J.; Qin, J.; Balke Wisinger, N.; Wang, H.; Maksymovych, P.; Wu, W.; Gupta, S. K.; Ye, P. D., Room-Temperature Electrocaloric Effect in Layered Ferroelectric CuInP2S6 for Solid-State Refrigeration. *ACS Nano* **2019**, *13* (8), 8760-8765.
16. Neumayer, S. M.; Tao, L.; O'Hara, A.; Brehm, J.; Si, M.; Liao, P.-Y.; Feng, T.; Kalinin, S. V.; Ye, P. D.; Pantelides, S. T.; Maksymovych, P.; Balke, N., Alignment of Polarization against an Electric Field in van der Waals Ferroelectrics. *Physical Review Applied* **2020**, *13* (6), 064063.
17. Scott, J. F., A comparison of Ag- and proton-conducting ferroelectrics. *Solid State Ionics* **1999**, *125* (1), 141-146.
18. Neumayer, S. M.; Tao, L.; O'Hara, A.; Susner, M. A.; McGuire, M. A.; Maksymovych, P.; Pantelides, S. T.; Balke, N., The Concept of Negative Capacitance in Ionically Conductive Van der Waals Ferroelectrics. *Advanced Energy Materials* **2020**.
19. Kresse, G.; Furthmüller, J., Efficient iterative schemes for ab initio total-energy calculations using a plane-wave basis set. *Physical Review B* **1996**, *54* (16), 11169-11186.
20. Blöchl, P. E., Projector augmented-wave method. *Physical Review B* **1994**, *50* (24), 17953-17979.
21. Kresse, G.; Joubert, D., From ultrasoft pseudopotentials to the projector augmented-wave method. *Physical Review B* **1999**, *59* (3), 1758-1775.
22. Perdew, J. P.; Burke, K.; Ernzerhof, M., Generalized gradient approximation made simple. *Physical Review Letters* **1996**, *77* (3865), 3865.
23. Becke, A. D.; Johnson, E. R., A density-functional model of the dispersion interaction. *The Journal of Chemical Physics* **2005**, *123* (15), 154101.
24. Grimme, S.; Ehrlich, S.; Goerigk, L., Effect of the damping function in dispersion corrected density functional theory. *Journal of Computational Chemistry* **2011**, *32* (7), 1456-1465.

SUPPORTING INFORMATION

I. Current at the beginning and end of DC voltage pulses

We investigate the current at the beginning (Fig. S1(a)) and end (Fig. S1(b)) of the DC voltage pulse. When the DC voltage pulse is turned on, ferroelectric switching events are visible as current peaks (Fig. S1(a)) and indicate the poling process of the capacitor. The corresponding total switched polarization is shown in Fig. S1(c). It is approximately between -8 and $-10 \mu\text{C}/\text{cm}^2$, which is about twice the reported remnant polarization and therefore indicates switching of the polarization vector from $-c$ to $+c$ orientation. This behavior is expected since the measurements are performed sequentially and the last applied voltage during the fast voltage sweeps is of positive polarity (Fig. 2(a)). In addition, currents appearing at the end of the pulses are also observed and are strongly dependent on the DC pulse duration (Fig. S1(b)). After pulses of 4, 10 and 20 ms duration, that do not activate ionic currents, I decreases to zero when the voltage pulse is turned off. If ionic currents are activated, at the end of the 100, 200 and 400 ms pulses, a positive current peak appears, corresponding to a total switched polarization of 0.4, 2, and $5.7 \mu\text{C}/\text{cm}^2$, respectively (Fig. 2(c)). For 500 ms and 600 ms, negative current peaks indicate a change in polarization of -3.5 and $-2.7 \mu\text{C}/\text{cm}^2$. For 800 and 900 ms pulses, no clear current peaks are observed and large currents are still measurable after the voltage has been turned off, which we interpret as relaxation of the ionic current. We hypothesize that the switching currents at the end of the DC voltage pulse can be interpreted as the formation of domains. Large ionic currents introduce disorder but since the measurements are below the Curie temperature, the ordered ferroelectric state re-forms after the voltage pulse. At this point, it is unclear how this process unfolds, but the experimental data suggest it involves first the formation of positively oriented domains which transition into negatively oriented domains as the DC voltage pulses become longer and more disorder is introduced.

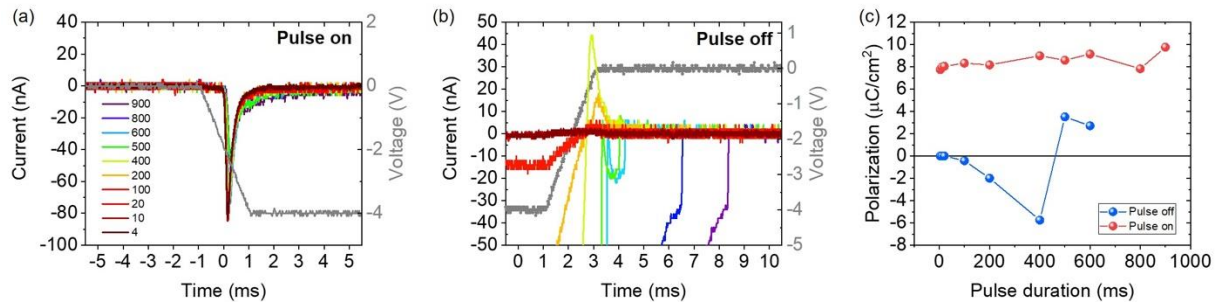


Fig. S1. (a) Current measured at the start of the square pulses. (b) Current measured at the end of the pulses. Time scales shifted to show the end of the pulse at the same time. (c) Polarization change during pulse on and off as a function of pulse duration.

II. Symmetric behavior at positive DC pulses

While negative DC pulses lead to negative currents in subsequent triangular pulses, the situation is symmetric for positive set pulses. In this case, positive DC pulses lead to positive ionic currents during the DC pulse and the positive part of the triangular voltage sweep (Fig. S2)

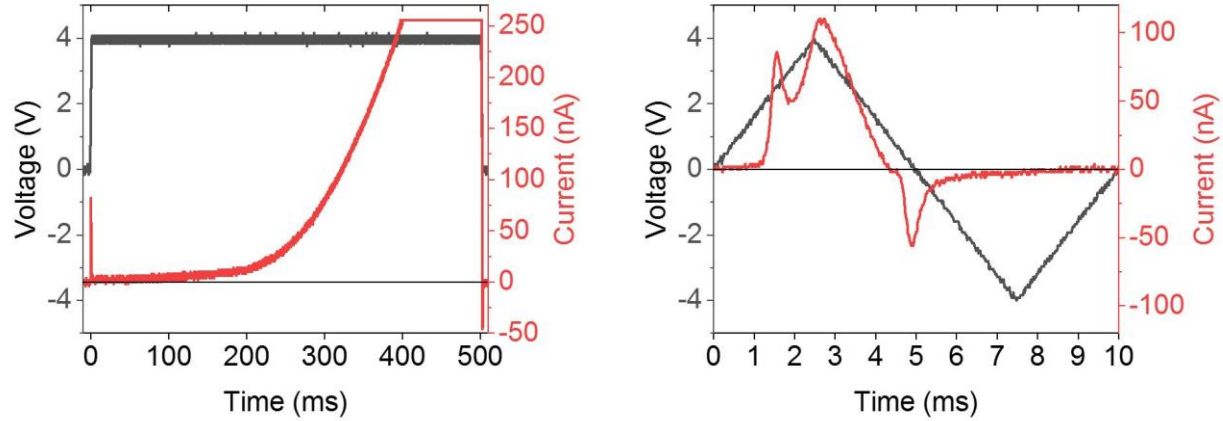


Fig. S2. Current during positive set pulse of 500 ms (left) and subsequent triangular voltage sweep (right).

III. Separation of ionic and polarization switching current

In order to separate the ionic and ferroelectric switching current, the total current is plotted as function of time and is fitted using 4 Gaussian distributions. Where the current is outside the current-measurement range, the fit provides an extrapolation of the ionic current, which is shown in the main text.

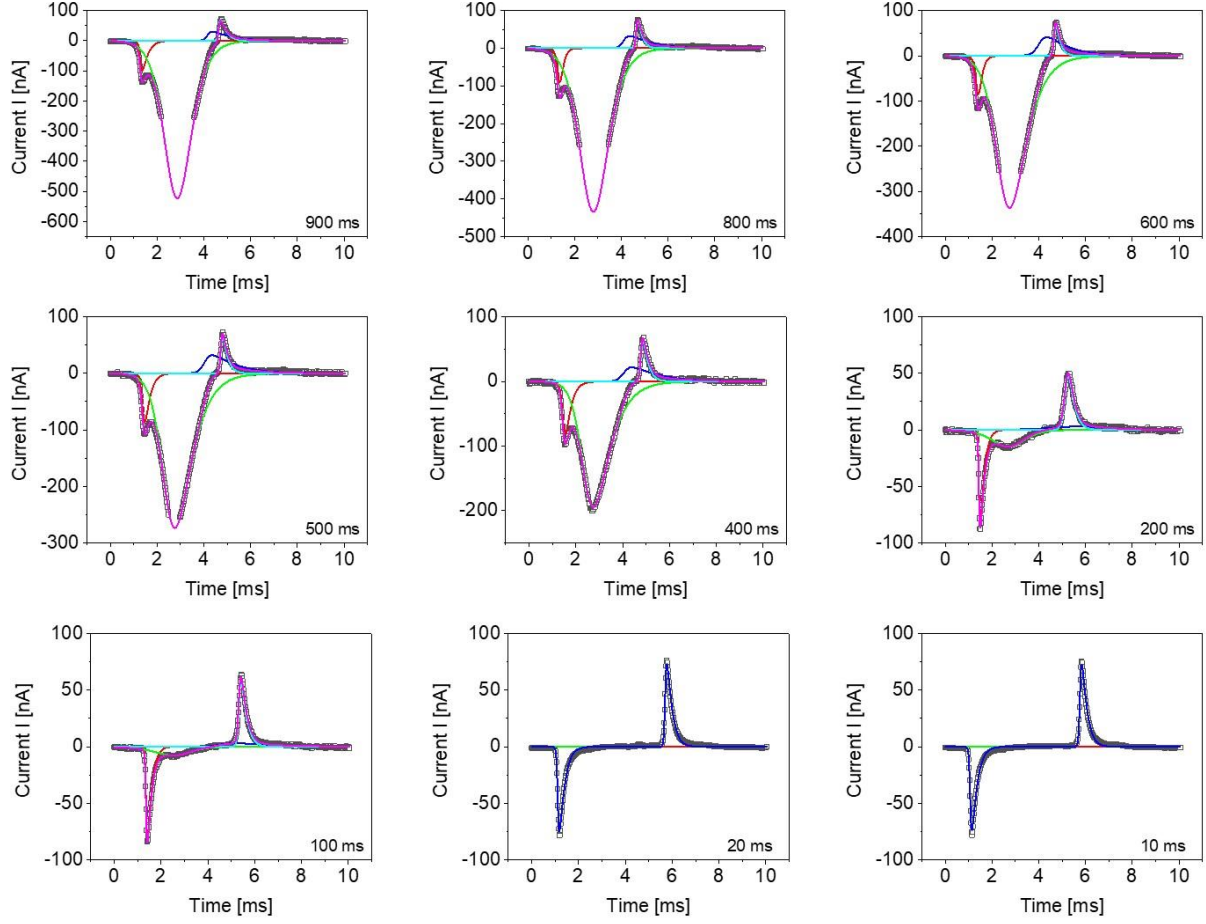


Fig. S3. Four-peak fitting of currents measured during the triangular voltage sweep to differentiate between ionic currents and the two polarization switching peaks at negative and positive voltages. The purple (100 ms to 900 ms) and blue (10 ms and 20 ms) curves show the overall fit. The additional peak in blue (400 ms to 900 ms) is an ionic contribution similar to the current peaks observed when longer DC voltage pulses are turned off.

III. Ionic current, ionic charge, and corresponding CIPS layer number

Here we explain how to calculate the ionic charge and the corresponding number of CIPS layers under the electrode that are necessary to provide the amount of charge required for the measured ionic currents. These calculations do not refer to the total number of CIPS layers across the entire sample thickness. The integral of the fitted ionic current contribution is used to determine the ionic charge Q_i . We assume that each Cu can take one electron according to $\text{Cu}^+ + e^- \rightarrow \text{Cu}$ accounting for a charge of $1.6022 \cdot 10^{-19}$ As. The amount of charge per CIPS layer is calculated by considering the number of unit cells in one layer under the electrode area ($20 \times 20 \mu\text{m}^2$) using cell parameters $a=6.11542 \text{ \AA}$ and $b=10.58783 \text{ \AA}$ with two Cu ions being present in each layer per these unit cell dimensions. We obtain a charge per CIPS layer of Q_{layer}

≈ 0.198 nC. The number of layers needed to provide the ionic charge is then the ionic charge divided by the layer charge.

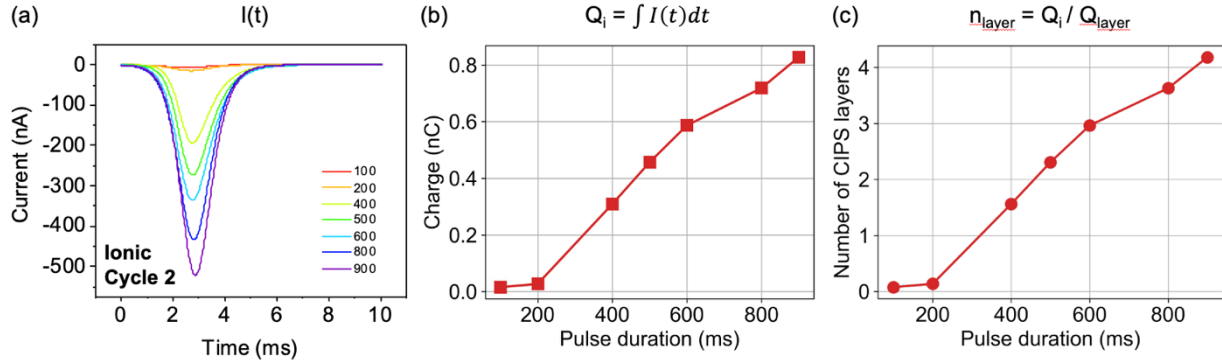


Fig. S4. (a) Ionic current, (b) ionic charge Q_i and (c) the number of CIPS layers needed to provide the ionic charge as function of DC voltage pulse duration.

IV. Polarization hysteresis area analysis

The area of the P(V) loops in Fig. 2(c) corresponds to an energy. Fig. S5 provides the loop area in units of energy as function of DC voltage pulse duration.

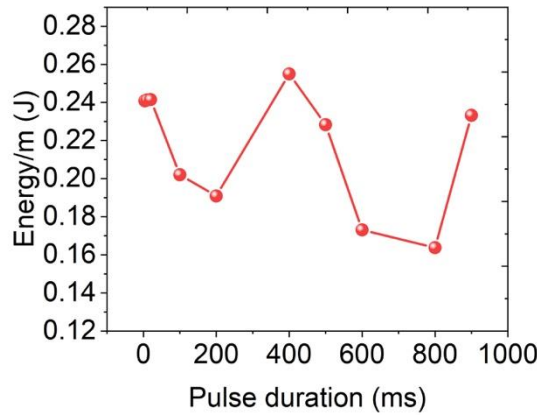


Fig. S5. Work as a function of DC voltage pulse duration calculated from the area of the polarization vs voltage loops in Fig. 2(c).

V. Ionically induced polarization changes as function of cycle number

To investigate the persistence of changes in ferroelectric and ionic behavior initiated by the DC voltage pulses, we probed currents during 10 triangular cycles that follow square pulses of 20 ms, 500 ms and 1000

ms at -6 V (Fig. S6(a)) on a virgin capacitor sample. The CIPS layer in this sample of ~420 nm was thicker than the previous sample shown in Fig. 1, which is why a higher voltage of 6 V was selected. The 20 ms pulse does not result in measurable ionic currents and only one switching peak is measured, whereas 500 ms and 1000 ms pulses result in ionic currents up to -40 nA and -160 nA, respectively (Fig. 7). After the 20 ms pulse, typical ferroelectric switching current peaks are measured during all of the 10 subsequent triangular cycles (Fig. S6(b)). Ionic currents appear during triangular cycles after the 500 ms (Fig. S6(c) and (d)). The first 5 cycles show ionic currents at negative V in addition to the ferroelectric switching currents. The ionic-current contribution decreases as a function of cycle number and vanishes at cycle #6. At a longer DC pulse of 1000 ms, which activates a higher ionic current, the ionic behavior impacts all switching cycles, albeit to a lesser degree at later cycles (Fig. S6(d)). Therefore, the maximum ionic current during triangular V sweeps is a function of both DC-voltage-pulse duration and cycle # (Fig. S6(e)). The longer the pulse, the higher the ionic current, which decreases exponentially with every cycle. If Cu ion accumulation under one electrode can be ascribed to the fast ionic current component, the decrease of ionic current as function of cycle number can be explained by spontaneous Cu redistribution based on the induced concentration gradient, which would increase the distance between Cu ions and the electrode and, therefore, reduce the fast ionic current component. The DC voltage pulse strongly affects the positive coercive voltage V_c^+ , which decreases with increasing DC voltage pulse duration but is relatively unchanged for subsequent cycle numbers (Fig. S6(f)). V_c^- on the other hand, is approximately constant around 4 V. This observation is consistent with the behavior shown in Fig. 2(e), where V_c^+ changes more significantly with increasing pulse duration than V_c^- . Moreover, we can conclude that ionic behavior activated by long DC pulses has a lasting impact on V_c^+ , i.e., on polarization switching, even in the absence of ionic currents at later cycles. It should be mentioned that the results in Fig. S6 and Fig. 2 are not directly comparable since they were conducted on different capacitors with different coercive voltages and different values of ionic current.

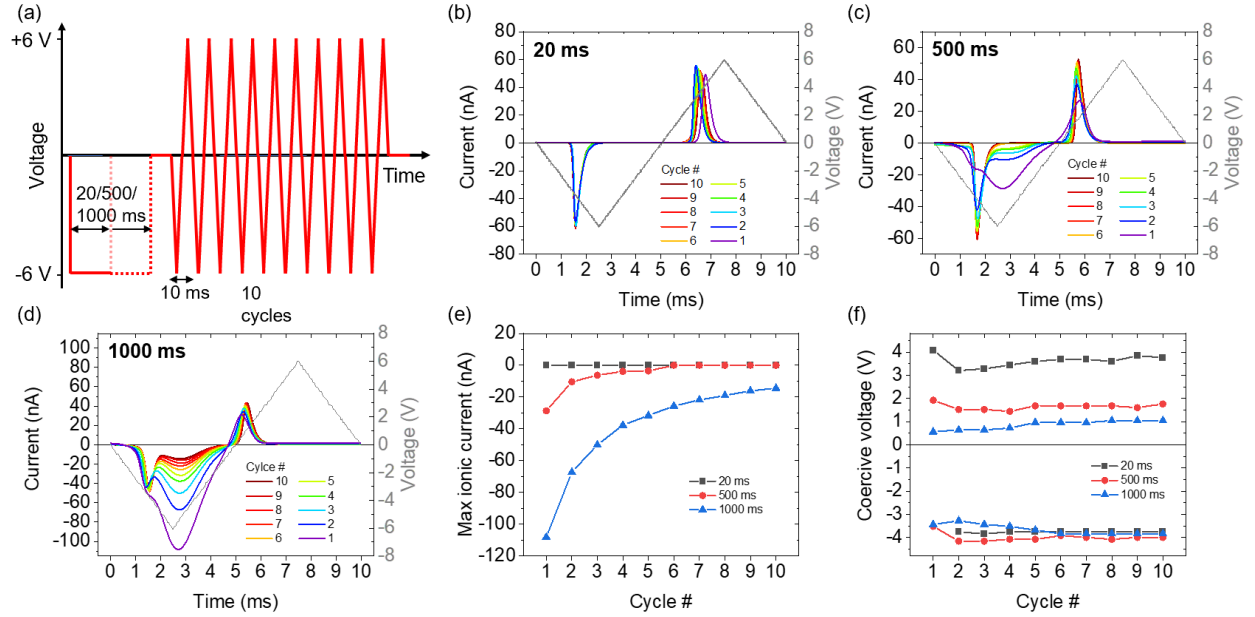


Fig. S6. (a) Scheme of waveform consisting of a -6V square pulse of either 20, 500 or 1000 ms followed by 10 triangular cycles of 10 ms duration. Current during the triangular cycles after (b) 20 ms, (c) 500 ms and (d) 1000 ms square pulses. (e) Maximum ionic current during triangular cycling after 20, 50, and 1000 ms pulses. (f) Positive and negative coercive voltages for all 10 cycles after 20, 50, and 1000 ms pulses.

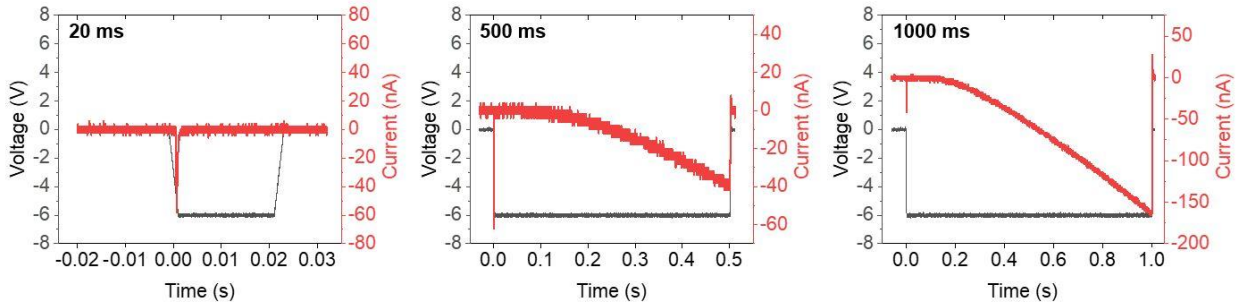


Fig. S7. Current during square DC voltage pulses of 20 ms, 500 ms and 1000 ms duration.

VI. Density of states calculations

In order to understand how the migration of copper affects the electronic structure of the system, we perform a layer-by-layer analysis of the density of states for each polarization state of the Ni/*m* InP₂S₆/*n* CuInP₂S₆/Cu/Ni system, shown in Fig. S8. The outermost layers (L1 and L6) are always metallic regardless of Cu content due to contact doping with the Ni contact. Initially (Fig. S8(a)), the middle four layers (L2, L3, L4 and L5) are insulating regardless of polarization state. However, after one or more layers of Cu have moved across the gap, there are now layers of InP₂S₆. InP₂S₆ can be considered either as Cu-deficient

CuInP_2S_6 or In-deficient $\text{In}_{4/3}\text{P}_2\text{S}_6$. Being heavily cation deficient in either perspective indicates that the InP_2S_6 layers are likely to be metallic. We confirm this via the density of states for InP_2S_6 in Fig. S9 and show a comparison to stoichiometric $\text{In}_{4/3}\text{P}_2\text{S}_6$ which is not metallic.

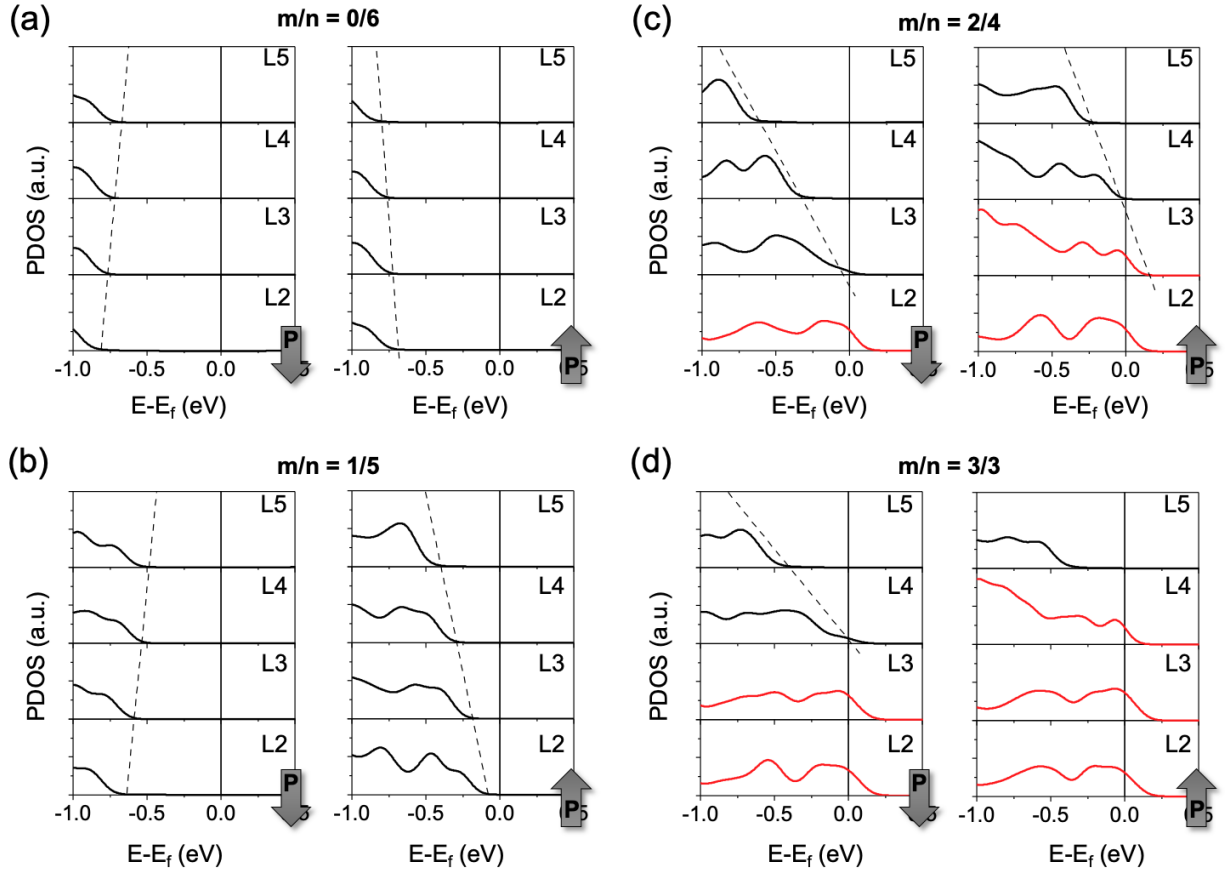


Fig. S8. Layer projected density of states projected for the $n\text{-CuInP}_2\text{S}_6/m\text{-InP}_2\text{S}_6$ system with (a) $m/n=0/6$, (b) $m/n=1/5$, (c) $m/n=2/4$, (d) $m/n=3/3$ for downward and upward oriented polarization, respectively. See Fig. 3 in the main text for atomistic structures. Electrically insulating layers are drawn in black, conductive layers are drawn as red lines. Layers L1 and L6 are omitted as they are fully metallic due to contact doping in all cases.

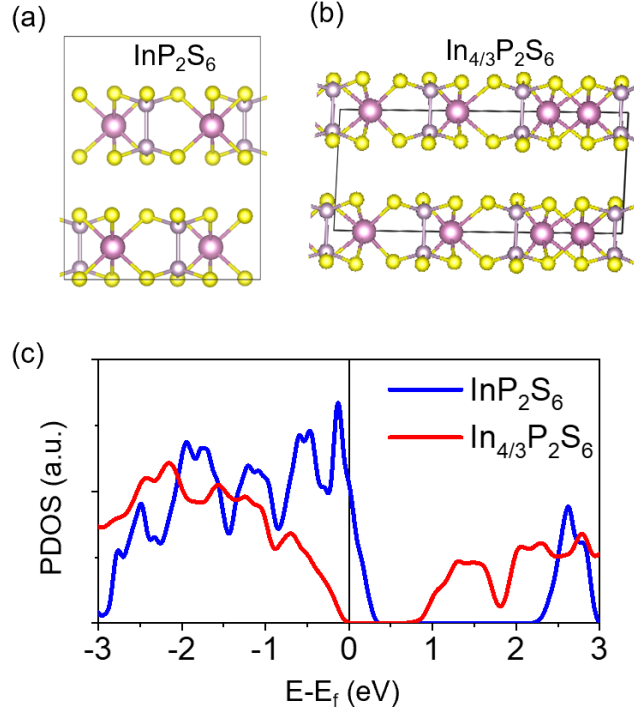


Fig. S9. Structures of (a) InP_2S_6 , that corresponds to the structure of CuInP_2S_6 in which all Cu atoms are missing, and (b) $\text{In}_{4/3}\text{P}_2\text{S}_6$. (c) Density of states of InP_2S_6 and $\text{In}_{4/3}\text{P}_2\text{S}_6$.

VII. Determination of internal electric field and polarization from DFT

Both the ferroelectric polarization and the movement of Cu atoms create internal electric fields of varying strength which manifest in a gradient of the valence-band edge position of each layer (*i.e.*, band bending). The black dashed line in Fig. S8 is placed connecting the valence-band edges in the insulating layers. The slope of this curve is indicative of the electric field value. In Fig. S10(a), we show all valence band edges for each of the cases. The sign of the slope (positive or negative) refers to the direction of internal electric field (up or down). These are the fields that are then plotted in Fig. 4(b) in the main text and indicate the build-up of an internal field caused by the ionic migration of Cu atoms.

The value of the spontaneous polarization for each slab is shown in Figure S10(b). The polarization is estimated by averaging the Cu displacement relative to the mid-layer centrosymmetric plane for each insulating layer of a given slab and comparing it to the nominal bulk values for a given displacement. The black dash line is the polarization as a function of Cu displacement in a periodic CIPS.

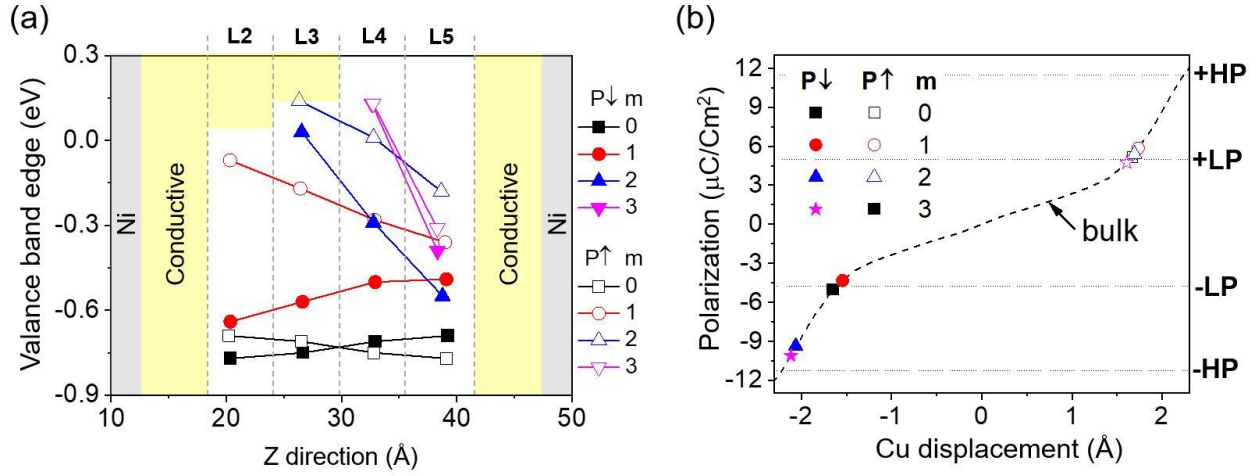


Fig. S10. (a) Valence-band edge of each insulating layer in each of the considered n/m configurations, according to PDOS in Figure S8. (b) Estimated polarization in each state according to the average Cu displacement. The black dash line is the polarization as a function of Cu displacement in a periodic CIPS. The horizontal blue dashed lines indicate the polarization values for the bulk polarization states.